In-plane distribution in mixtures of cationic and anionic surfactants†

David Carrière,*[a] Luc Belloni,[a] Bruno Demé,[b] Monique Dubois,[a] Claire Vautrin,[a] Annette Meister[c] and Thomas Zemb[ad]

Received 23rd June 2009, Accepted 20th August 2009
First published as an Advance Article on the web 13th October 2009
DOI: 10.1039/b912286a

Mixtures of cationic and anionic surfactants, also called "catanionic" mixtures, self-assemble into aggregates which show a rich variety of morphologies in the nanometre to micron range controlled by the molar ratio between surfactants. At the molecular scale, little is known about the local distribution of surfactants in the bilayer. Here, we determine the in-plane distribution of the cationic and anionic surfactants in catanionic bilayers using neutron scattering and the contrast matching technique. The coexistence of two different in-plane orders is experimentally demonstrated: both surfactants share a common two-dimensional hexagonal lattice with a long-range order, but the distribution of alternate (+) and (−) charged head groups shows only a two-dimensional liquid-like local order. Comparing experiments and Monte-Carlo simulations, we establish that this lateral liquid order is attenuated by the counterions of the bilayers, but is less than expected in a mean-field approach. This demonstrates that electrostatic interactions participate in, but do not completely determine, the local distribution of surfactants of opposite charge in the bilayer.

Introduction

Aqueous mixtures of surfactants of opposite charge, also called "catanionic" mixtures, self-assemble into mixed micelles rich in either surfactant or into flatter aggregates when the surfactant composition is sufficiently balanced to allow significant reduction in curvature: lamellar phases, nano- and micro-discs, vesicles, bicontinuous structures, *etc.*[1–10] This was first exploited by Jokela *et al.* who used the phase diagram for quantitative measurement of hydration forces in the absence of salt.[1] As far as general behavior is concerned, the mixed surfactant aggregates are well understood in terms of equilibrium composition, curvature, stability, size distribution, *etc.*, leading to good descriptions and reasonable predictions at the scale of the aggregate (nanometre to micrometre).[11–19] By contrast, there is currently little experimental data about the catanionic mixtures at the molecular scale, although some important and intriguing behaviors have been hypothesized: for instance, two-dimensional co-crystallization in the bilayer at a preferential ratio and segregation of the excess have been invoked to describe the formation of facetted vesicles.[17,20,21] This is compatible with the observation of a very preferential fatty acid : cationic ratio = 2 : 1 at which the interaction energy between surfactants is high enough to prevent extraction of the water-soluble cationic surfactant by dialysis,[22] leading to the formation of vesicles suitable for sustainable encapsulation of added solute as well as for "self-encapsulation" of the surfactant counterions released upon bilayer formation.[23] Assuming the formation of a highly cohesive crystal with a definite composition would account for such a preferential ratio. However, no direct structural evidence is available yet. Additionally, Monte-Carlo and molecular dynamics simulations of planar and cylindrical mixed micelles do not predict such preferential compounds, but rather a lateral phase separation between both surfactants leading to nanometric patterns originating from the competition between electrostatic interactions that favor mixing and tail incompatibility that favors segregation.[24,25] Direct experimental characterization of the in-plane organization in catanionic bilayers with molecular resolution is therefore required to understand their macroscopic behavior, *e.g.* morphology, stability, *etc.*

Here, we use small-angle neutron scattering with contrast matching techniques to investigate selectively the relative in-plane organization of both surfactants. As opposed to X-ray scattering, neutron scattering can provide contrast between surfactants if one of them is deuterated. This property has been used several times in other characterizations of catanionic systems, *e.g.* bulk *vs.* aggregate composition[26–28] or size and morphology characterization.[18,27,29–35] However, these studies exploit the mean contrast of the mixed micelles or bilayers. In the work presented here, it is rather the contrast between both surfactants which is used to extract information about their lateral distribution in the bilayer. We used for this study lamellar phases prepared from mixtures of perdeuterated myristic acid ($C_{13}D_{27}COOH$) and cetyltrimethylammonium hydroxide (CTA^+OH^-) in D_2O and stabilized by HCl or CTACl in small amounts ($0.05 < Cl^-/CTA^+ < 0.20$). As the hydroxide counterions are neutralized by the protons of myristic acid or HCl, the ions present in solution are only counterions of the bilayers, as opposed to added salt. There is therefore little screening of the

[a]*CEA, IRAMIS, SIS2M, LIONS, F-91191 Gif-sur Yvette Cedex, France. E-mail: david.carriere@cea.fr; Fax: +33 (0)1 69 08 66 40; Tel: +33 (0)1 69 08 54 89*
[b]*Institut Laue-Langevin, B.P. 156, F-38042 Grenoble Cedex 9, France*
[c]*Martin-Luther-Universität Halle-Wittenberg, Institut für Physikalische Chemie, D-06108 Halle, Germany*
[d]*CEA, ICSM, UMR 5257 CEA/CNRS/UM2/ENSCM, F-30207 Bagnols sur Cèze, France*

† Electronic supplementary information (ESI) available: Color snapshot of Monte-Carlo simulation with imposed full dissociation (associated to Fig. 6), color snapshot with imposed zero surface charge density (associated to Fig. 7). See DOI: 10.1039/b912286a

electrostatic interactions. At room temperature, these lamellar phases are in the gel state,[10,36] which quenches the lateral diffusion of both surfactants in the bilayer and avoids time-average of the scattering length density. We show that in these conditions, small-angle neutron scattering (SANS) allows us to demonstrate that the surfactant molecules are distributed on a hexagonal network, and that locally the molecules of opposite charge show only a liquid order with a range of a few tens of ångströms. No superstructure is observed, nor predicted by Monte-Carlo simulations taking into account the dielectric water–tail interface. The influence of counterion screening on this local order is lower than expected, which indicates that the interaction between different surfactants is higher than predicted by a purely electrostatic mean-field approach.

Experimental

Preparation of the catanionic mixtures

Perdeuterated myristic acid ($C_{13}D_{27}COOH$, Aldrich) and deuterated water (Eurisotop) were used as such. Cetyltrimethylammonium hydroxide (CTAOH) was either obtained from a freeze-dried commercial solution (Fluka) or from ion-exchange on a resin in hydroxide form (Dowex) of the halide forms CTACl or CTABr (Fluka). CTAOH was handled under an inert atmosphere throughout the preparation. The amount of residual anions was in the 5–20% range, as determined by capillary electrophoresis (Waters). The stabilization of the L_β phase requires the presence of 5–20% residual halide ions.[36] The use of $CTA(OH)_xCl_{1-x}$ obtained either from an incomplete exchange on resin or from mixing CTAOH and CTACl gave identical results. The catanionic lamellar phases were prepared by mixing $CTA(OH)_xCl_{1-x}$ and myristic acid (Fluka, recrystallized twice from hot acetonitrile) at a total weight concentration in water in the 10–20% range. All products were handled under an inert atmosphere. The aqueous mixture was stirred until the complete dissolution of the myristic acid crystals, heated at 60 °C and cooled down at room temperature.

WAXS

Wide angle X-ray scattering (WAXS) experiments were performed with a molybdenum source ($\lambda = 0.711$ Å) using a home-built pinhole-geometry camera[10] and recorded on an image plate with a typical exposure time of 1 h.

Small-angle neutron scattering

Diffraction and small-angle neutron scattering (SANS) measurements were performed on D16 and D22 at the Institut Laue-Langevin, Grenoble, France. Neutron contrast between both surfactants was achieved by using *d*-27 perdeuterated myristic acid (Aldrich) and deuterated water for the catanionic preparations instead of the hydrogenated forms.

Theory and simulation

Monte-Carlo simulation

Cationic B^+ and anionic A^- surfactant heads in given numbers N_A, $N_B = N - N_A$ occupy all N sites of a 2D hexagonal lattice (rectangular cell with periodic boundary conditions). A Monte-Carlo trial move consists to exchange the positions of two different charges and to accept them according to the counterion-average mean-field electrostatic potentials described below (no explicit description of the counterions in this simulation) and to the standard Metropolis probability $\min(1,\exp(-(U_{new} - U_{old})/kT))$ (U represents the energy of the configuration). For such short-range screened potentials, the minimum image convention is sufficient. Note that, since all sites are occupied, it is only the contrast between the different potentials that governs the order; a binary mixture with potentials v_{AA}, v_{AB}, and v_{BB} is equivalent to a system of N_A A molecules interacting with $v_{AA} - 2v_{AB} + v_{BB}$. As far as the electrostatic coupling is concerned, a ± 1 system is equivalent to a 2/0 one.

When the weakness of the myristic acid is investigated, the system contains a third component, AH, of charge 0 (protonated acid). The fraction α of A^-/A is either fixed during the simulation (canonical ensemble) or is allowed to vary (grand-canonical). In the latter case, the $pK - pH$ difference is imposed, and switches between the A^- and AH forms on the same lattice site are investigated according to it. For instance, the transition $A^- \rightarrow AH$ is considered (with the same frequency as the inverse one) by randomly choosing one of the A^- sites and accepting the switch with the probability $\min(1,10^{pK-pH}N_{A^-}/(N_{AH} + 1)\exp(-(U_{new} - U_{old})/kT))$. For simplicity, we ignore the fact that this transition may modify the ionic composition of the medium against the layer and the screening of the electrostatic potentials. The interest of this grand-canonical approach is that it is able to determine the averaged degree of dissociation, it allows for fluctuations of this degree and it accounts for charge regulation effects that tend to release the electrostatic coupling and favor overall neutral configurations. The price to pay is that it requires an *a priori* value for the equilibrium constant pK. In the absence of any knowledge of this interface quantity, we have chosen to use the bulk value $pK = 6$. In practice, as long as the simulation cell is large (thermodynamical limit), the fluctuations authorized in the grand-canonical simulation do not modify the scattering spectra obtained in the canonical one (performed at the same average α).

The 2D structure factors (in-plane q) are accumulated along the simulation. The 3D scattered intensity is finally obtained by multiplying by the form factor of the surfactant molecules (seen as cylinders with a three-step scattering length density profile along the long axis), by multiplying by a simple bilayer–bilayer paracrystalline structure factor along the perpendicular direction (the details of which are unimportant in the present study at large q), and by powder-averaging.

Counterion-averaged head–head potentials

The interactions between charged heads localized on the same side of a bilayer have been modeled as screened electrostatic interactions between point charges at a dielectric (water–alkyl chains) interface. The screening comes from the aqueous medium above the interface that contains the counterions which neutralize the overall charge density of the layer (no added salt). The counterionic fluid is treated at the mean-field level. The

starting point is the non-linear Poisson–Boltzmann (PB) equation which governs the counterion density profile in a salt-free aqueous region against a charged planar plate of uniform charge density Σ, $\rho(z) = 2\pi L_B \Sigma^2/(1 + z/L)^2$ where L_B is the Bjerrum length and L is the Gouy–Chapman length that characterizes the thickness of this profile:

$$L = \frac{1}{2\pi L_B \sum} \tag{1}$$

When two point-like charges z_i and z_j (in principle, infinitively small; in practice, taken as the head monovalent charges) are added at the interface, $z = 0$, their potential of interaction $v_{ij}(r)$ as a function of their in-plane separation r is obtained by linearizing the PB equation around its uniform solution and expressed as an inverse 2D Fourier transform:[37]

$$\frac{v_{ij}(r)/kT}{z_i z_j L_B} = f(r) = 2\int_0^\infty \frac{1 + (kL)^{-1}}{1 + (kL)^{-1} + (kL)^{-2} + \eta\left(1 + (kL)^{-1}\right)} J_0(kr)\,\mathrm{d}k \tag{2}$$

where $\eta \equiv \varepsilon_{oil}/\varepsilon_{water}$ represents the dielectric discontinuity, with usually $\eta \ll 1$.

At short separations ($r \ll L$), $f(r)$ behaves as $2/r$. In that regime, the counterion cloud has no effect on the direct coulombic interaction between the two test particles and one recovers the bare coulombic potential (the factor 2 accounts for the interaction with electrostatic images). In the opposite regime of large separations ($r \gg L$), f presents the following asymptotic law, derived by expanding the fraction in the integrand in powers of k, which accounts for the counterion screening effect:

$$f(r) \approx 18\frac{L^4}{r^5} + 2\eta\frac{L^2}{r^3} \tag{3}$$

The first, original r^{-5} law dominates, except at very large separation ($r \gg L/\sqrt{\eta}$) where the second r^{-3} law, which accounts for the propagation of the field lines through the organic medium and can be called an effective dipole–dipole (head–counterion) interaction, takes place. In practice, this cross-over distance is very large and can be safely ignored. For the very same reason, the finite thickness of the organic bilayer and the coupling between upper and lower monolayer heads have been neglected. So, the potential law varies between r^{-1} and r^{-5} regimes.

An analytical interpolation function, which accounts for next order terms in the expansion, has been used during the Monte-Carlo simulations:

$$f(r) = \frac{2}{r}\frac{1}{1 + 1.209(r/L) + 0.462(r/L)^2 + (r/L)^4/9} \tag{4}$$

Examples of resulting pair potentials in the absence of screening salt for various Gouy–Chapman lengths are shown in Fig. 1. For $L = 10$ Å, the potential equals k_bT at a distance of $r = 6.9$ Å, which corresponds to a position intermediate between the second and third closest neighbor on the hexagonal network of surfactants. The magnitude of the interaction decreases accordingly as the Gouy–Chapman length decreases.

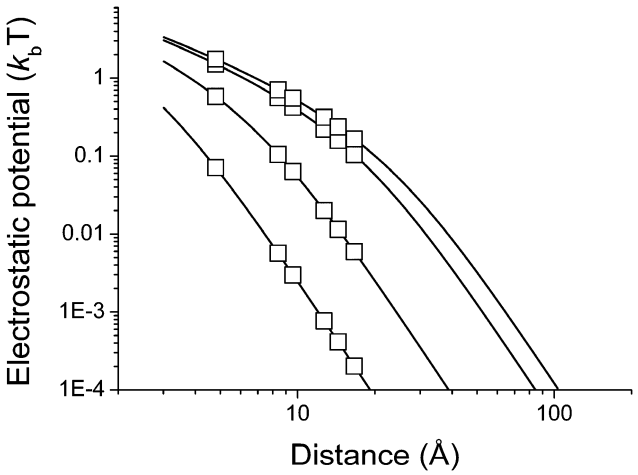

Fig. 1 Electrostatic pair potential on a charged plane delimiting a dielectric discontinuity ($\varepsilon_{oil}/\varepsilon_{water} \ll 1$), calculated with Gouy–Chapman lengths from top to bottom: $L = 10$ Å, 7.7 Å, 2.9 Å and 1.2 Å. The curves go from an r^{-1} to an r^{-5} law. The squares represent the distances of the six first neighbors on a hexagonal network with an area per chain of 20.5 Å^2.

Results and discussion

In a previous study, we have shown that aqueous solutions of cetyltrimethylammonium myristate ion pairs obtained from an equimolar mixture of myristic acid ($C_{13}D_{27}COOH$) and cetyltrimethylammonium hydroxide (CTA^+OH^-) transiently form bilayers that precipitate into a poorly hydrated crystal due to the lack of electrostatic repulsions. However, addition of HCl or CTACl in small amounts ($0.05 < Cl^-/CTA^+ < 0.20$) to the system equivalently results in stabilization of swollen lyotropic lamellar phases by charging the bilayers.[36] Although more subtle dissociation effects come into play, this can be roughly summarized as:

$$(C_{13}D_{27}COO^-CTA^+) + xH^+Cl^- \rightarrow (C_{13}D_{27}COOH_x)(C_{13}COO^-)_{1-x}CTA^+ + xCl^- \tag{5}$$

At Cl^- contents higher than $x = 0.20$, a small amount of H^+Cl^- originating from the partial dissociation of myristic acid screens out the electrostatic repulsion, and the bilayers collapse again.

Here, the mixed surfactant bilayers are formed upon mixing of perdeuterated myristic acid ($C_{13}D_{27}COOH$) and cetyltrimethylammonium, mainly under the hydroxide form ($CTA^+Cl_x(OH)_{1-x}$, $0.05 < x < 0.20$) in D_2O at various surfactant ratios. The molar fraction f of myristate molecules, either dissociated or not, is defined as:

$$f = \frac{n(\text{myristate})}{n(\text{myristate}) + n(\text{CTA})} \tag{6}$$

In the following, we focus on surfactant mixtures prepared with surfactant concentrations c typically higher than 10% weight in D_2O. The superimposition of neutron diffusion patterns measured in different configurations on the two instruments gives a complete view of the structure of the surfactant mixtures. A typical neutron scattering pattern, obtained for $f = 0.55$, is shown in Fig. 2. In the low-q range (3×10^{-3} Å$^{-1} < q < 0.4$ Å^{-1}) a series of up to 10 Bragg peaks at regular spacings in the 10^{-2} Å^{-1} to 10^{-1} Å^{-1} range are observed. This is

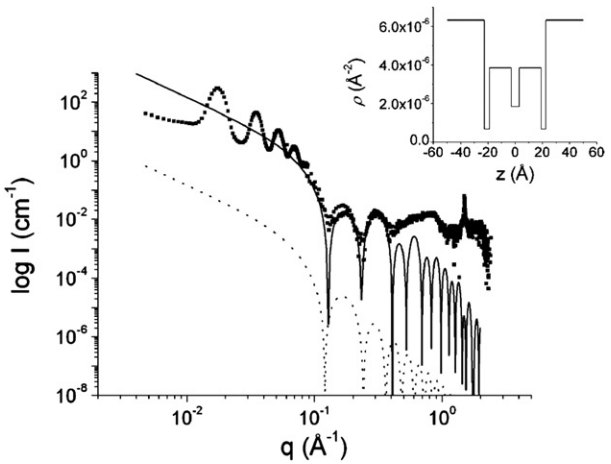

Fig. 2 SANS pattern of a CTAOH–perdeuterated myristic acid mixture in D_2O at a myristic acid molar fraction $f = 0.55$, $c = 13\%$ wt in D_2O. The dotted line is the form factor of a plane of thickness 52 Å. The full line is the form factor corresponding to the scattering length density profile shown in inset.

assigned to extremely swollen and ordered lamellar phases. The interlamellar distance is calculated from the spacings between the Bragg peaks, and varies in the range of 90 to 385 Å depending on f and the total surfactant concentration.

At the highest angles, a very narrow Bragg peak is not only observed at $q = 1.5$ Å^{-1} on the neutron scattering patterns, but also on the X-ray scattering patterns (Fig. 3). This peak is single and symmetric, which allows us to assign it to the (110) reflection degenerated with the (020) reflection in a hexagonal lattice.[22,38,39] In other words, it corresponds to an in-plane hexagonal packing of the alkyl surfactant chains. Several possible organizations of the chains are *a priori* compatible with such a pattern:[40]

(1) A "free rotator" phase, with a long-range hexagonal positional order of the molecules and freely rotating alkyl chains. However, this structure requires large mean areas per chain (>25 Å^2). In our case, the mean area per chain is 20.5 Å^2 only, as determined from:

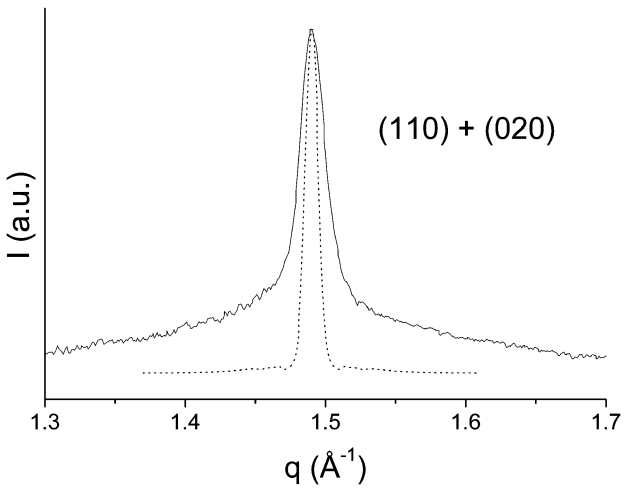

Fig. 3 WAXS pattern with (110) + (020) reflections of an equimolar mixture of myristic acid and $CTA(OH)_{0.8}Cl_{0.2}$, 15% wt in H_2O. Dotted line: direct beam.

$$A_c = \frac{2}{\sqrt{3}}\left(\frac{2\pi}{q_{110}}\right)^2 \quad (7)$$

Free rotator phases are therefore excluded in the present case.

(2) The most relevant structure is therefore an RII-type rotator phase, with locally orthorhombic (distorted-hexagonal) domains that are macroscopically averaged into a hexagonal symmetry due to orientational disorder of the domains. The resulting positional order is, however, high enough to allow the observation of a sharp peak (FWMH = 0.024 Å^{-1}, direct beam = 0.012 Å^{-1}).

At intermediate q ranges (0.1 Å^{-1} < q < 1 Å^{-1}), several broader peaks are observed on the neutron scattering patterns around $q = 0.18$ Å^{-1}, 0.32 Å^{-1} and 0.80 Å^{-1} (Fig. 2). The first two oscillations observed around $q = 0.18$ Å^{-1} and 0.32 Å^{-1} are assigned to the form factor of the bilayers forming the lamellar phase. The first correlation peak is well modeled by the form factor of a plane of thickness $2d$ with an homogeneous scattering length density, leading to a scattered intensity given by:[41]

$$I(q) = \frac{8\pi\Sigma}{q^2}\Delta\rho^2\left(\frac{\sin(qd)}{q}\right)^2 \quad (8)$$

where Σ is the specific area of the bilayers, with the bilayer thickness $2d = 52$ Å (Fig. 2, dotted line).

The position of the second correlation peak at $q = 0.32$ Å^{-1} is correctly captured by this simple model, but its intensity is strongly underestimated by about a factor of 10. A better description is given by assuming a distribution of scattering length density along the normal to the bilayer. If the bilayers are assumed symmetric along the midplane, and each monolayer is described by three slabs of different scattering length densities and thicknesses (inset in Fig. 2), then the scattered intensity is given by:[41]

$$I(q) = \frac{8\pi\Sigma}{q^2}\left(\sum_{i=1}^{3}(\rho_i - \rho_{i-1})\frac{\sin(qd_i)}{q}\right)^2 \quad (9)$$

where Σ is the specific area of the bilayers, ρ_0 the scattering length density of D_2O, ρ_i the scattering length density of the i-th layer and d_i the distance between the midplane of the bilayer and the boundary between the layers i and $i - 1$. A good agreement between the form factor and the two correlations at $q = 0.18$ Å^{-1} and 0.32 Å^{-1} is found with the scattering length density profile presented in the inset in Fig. 2 and Table 1 (Fig. 2, full line). The bilayer thickness is around 45 Å, which compares well with the thickness estimated from the length of the surfactants with little tilt in the bilayer. In addition, the mean scattering length density is close to that expected from the surface per chain and the chemical composition (3.16×10^{-6} Å^{-2} at $f = 0.55$), and the respective scattering length densities of each slab compare well with rough estimates of that expected for the heads, chains and tails (Table 1).

The surfactant molecules therefore assemble into catanionic "frozen" lamellar phases (L_β), with an average positional order of the chains that define a hexagonal lattice. The last feature is observed at intermediate angles (0.4 Å^{-1} < q < 1 Å^{-1}). In this medium angle range, a very broad correlation peak with a maximum around 0.8 Å^{-1} is observed. This peak is systematically observed, independently of the composition of the catanionic sample (magnified in the lin-lin plot of Fig. 4).

Table 1 Thicknesses d_i and scattering length densities ρ_i used for the form factor of the bilayer at $f = 0.55$, from an estimate of the SLD for the head, chain and tail regions

Layer	1 (head)	2 (chain)	3 (tail)
Composition estimate	fCOO + $(1-f)(CH_2)_3N(CH_3)_3$	$f(CD_2)_{12}$ + $(1-f)(CH_2)_{12}$	fCD_3 + $(1-f)CH_3$
d_i/Å	3.5	16	3
ρ_i^a/Å^{-2}	6.2×10^{-7}	3.9×10^{-6}	2.1×10^{-6}

[a] The scattering length densities were estimated from the sum of atomic scattering length and the volume $v_i = d_i A_c$.

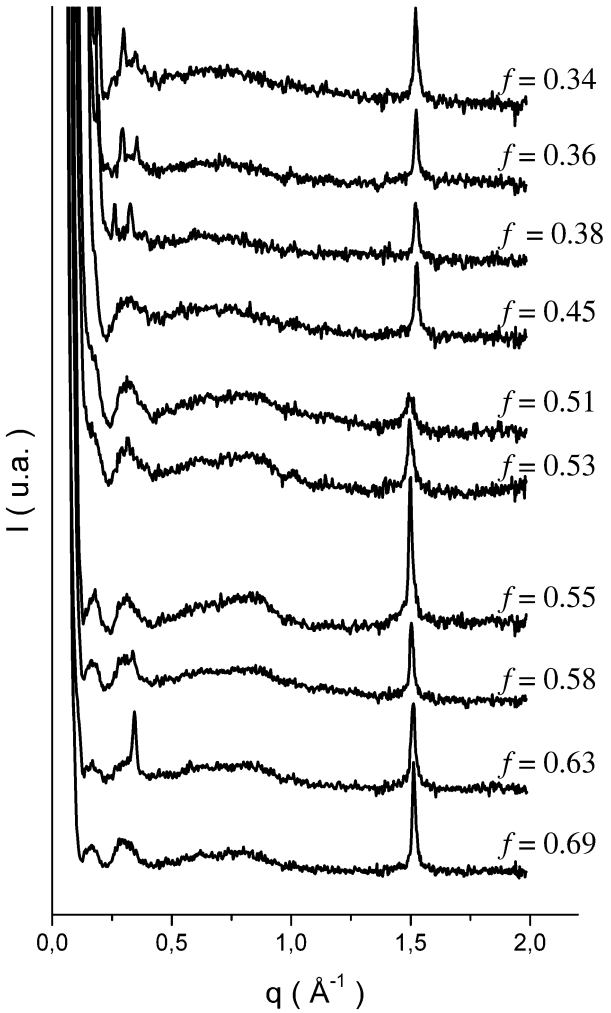

Fig. 4 Neutron diffraction patterns of cetyltrimethylammonium–perdeuterated myristic acid mixtures in D_2O with variable *d*-27 myristic acid molar fractions (*f*). The curves are shifted for convenience.

This broad correlation peak centered at $q = 0.8$ Å^{-1} is assigned to the in-plane organization of the two different surfactant chains. This local organization cannot be observed with WAXS due to the lack of electronic contrast between both surfactant chains, but is observed by neutron scattering after introduction of a scattering length density contrast between the two chains. This neutron scattering experiment allows discrimination between the two different in-plane orders, namely the hexagonal order between both surfactant chains (peak at 1.5 Å^{-1}) and the order between the CTA chains only (peak between 0.50 and 1 Å^{-1}). In the absence of correlations between deuterated chains

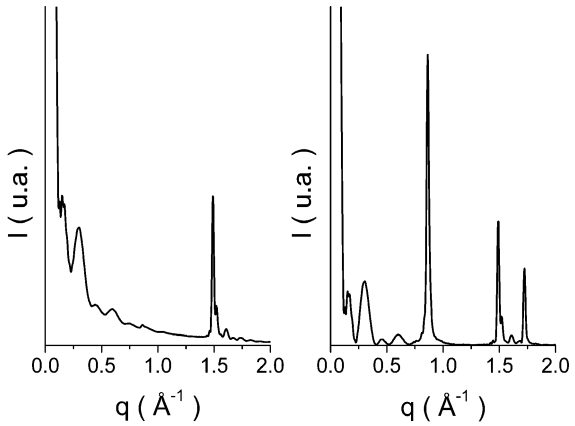

Fig. 5 Effect of the distribution of surfactants on the peak at 0.85 Å^{-1} in a catanionic membrane of composition $f = 2/3$; left: random lateral distribution of surfactants in the bilayer and right: (3×1) superstructure.

(*i.e.* a random distribution of surfactants onto the hexagonal network), the broad peak at intermediate *q* values is expected to cancel out (Fig. 5a). By contrast, a sharp peak is expected as correlations between surfactants of the same kind enhance. In the extreme situation where the CTA molecules would perfectly organize onto a superstructure, a sharp reflection is expected. For instance, a hexagonal (3×1) superstructure achieved with $r = 1/3$ or $r = 2/3$ would yield a peak at 0.83 Å^{-1} (Fig. 5b).

The two situations depicted in Fig. 5 are purely limit cases. Experimentally, only intermediate cases between superstructure and random lateral distribution are observed (Fig. 2 and 4), which demonstrates the existence of a liquid order of intermediate range between both surfactants. A first possible origin of this local order is the electrostatic interactions between heads of opposite charge. In order to check this hypothesis, the experimental neutron scattering patterns have been compared with the theoretical predictions given by Monte-Carlo simulations described previously. The simulations were performed with different assumptions regarding the dissociation of myristic acid ($\alpha = C_{13}D_{27}COO^-/[C_{13}D_{27}COOH + C_{13}D_{27}COO^-]$). In the first case, a full dissociation of myristic acid ($\alpha = 1$) is assumed. In this case, the Gouy–Chapman length is directly calculated from the structural charge density:

$$L = \frac{A_c}{2\pi L_B |1-2f|} \quad \text{for } \alpha = 1 \tag{10}$$

There is a good qualitative agreement between the experimental data and the patterns predicted by the Monte-Carlo simulations regarding the presence of the Bragg peaks and the two correlation peaks assigned to the form factor of the bilayer

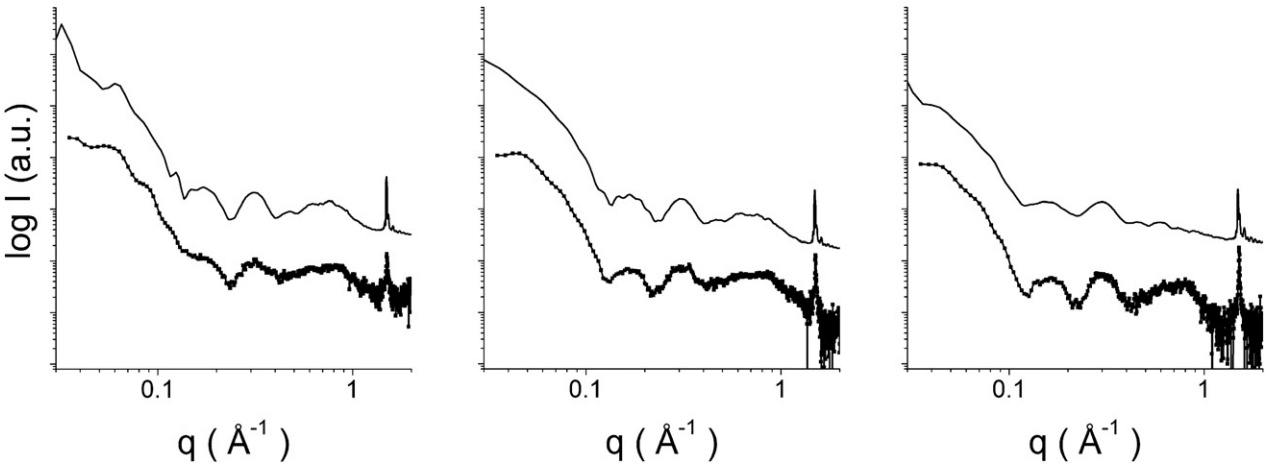

Fig. 6 Monte-Carlo simulations (top curves) and experimental neutron data (bottom curves), with $f = 0.53$, 0.58 and 0.68 from left to right, and a full dissociation of myristic acid giving $L = 7.7$ Å, 2.9 Å and 1.2 Å, respectively. Corresponding Monte-Carlo snapshots are provided as ESI†.

(Fig. 6 and ESI†). In addition, at $f = 0.53$ ($L = 7.7$ Å), the correlation peak around $q = 0.80$ Å^{-1} is correctly predicted in terms of position and magnitude (Fig. 6, left). The experimental pattern does not change significantly as f increases (Fig. 6, middle and right). By contrast, in the predicted patterns, the magnitude of the correlation peak assigned to the in-plane order decreases as the composition goes off-stoichiometry. This results from the decrease of the electrostatic interaction as the surface charge density increases. At $f = 0.68$, the correlation is even predicted to disappear, as a result of the smallness of the Gouy–Chapman length ($L = 1.2$ Å) which reflects a large screening of the electrostatic interactions by the counterions.

This underestimation of the liquid order, particularly at compositions far from stoichiometry, suggests that the effective charge is lower than the structural charge as estimated from the composition in anionic and cationic surfactant. Indeed, myristic acid behaves like a very weak acid, with a strong shift in pK_a.[36] A first-order approximation, validated by our grand-canonical Monte-Carlo simulations, assumes that charge regulation effects impose that the bilayer remains as close to electrostatic neutrality as possible, which gives:

$$\begin{aligned} \alpha &= 1 \quad \text{for } f < 0.5 \\ \alpha &= \frac{1}{f} - 1 \quad \text{for } f > 0.5 \end{aligned} \tag{11}$$

The Gouy–Chapman length would therefore tend to infinite values at all compositions and increase the magnitude of the electrostatic interactions. In practice, it is found that using moderately high values of L combined with a zero surface charge density in the Monte-Carlo simulations is sufficient to recover the presence of the correlation peak of the liquid order (Fig. 7, with $L = 10$ Å and ESI†), even far from stoichiometry.

This gives a realistic image of the in-plane distribution of both surfactants. The two-dimensional order can be further quantified in the Monte-Carlo simulation by extraction of the pair correlation functions (Fig. 8). They demonstrate that the liquid order in the plane propagates up to 10 Å, *i.e.* to the third neighbor in

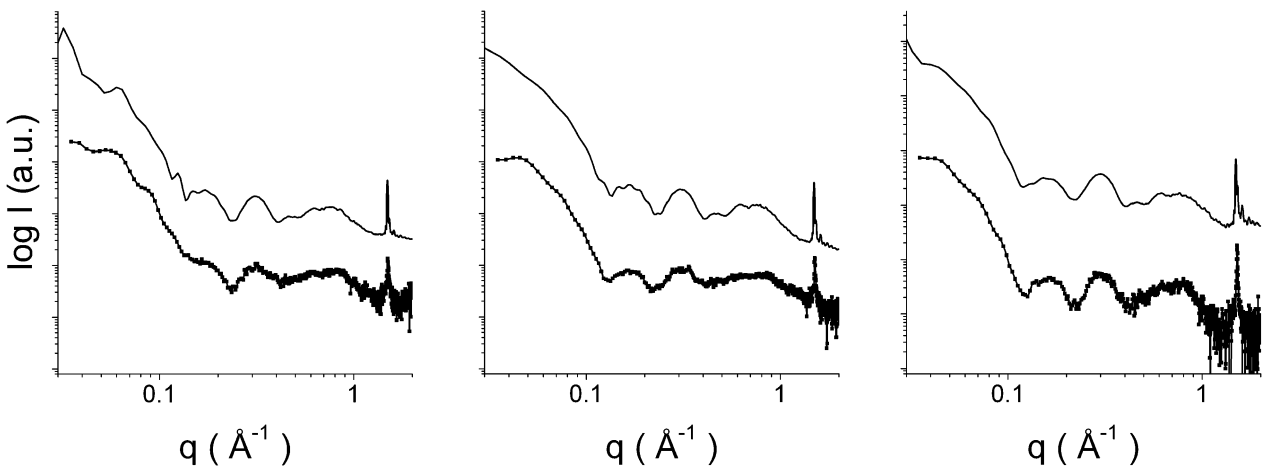

Fig. 7 Monte-Carlo simulations (top curves) and experimental neutron data (bottom curves), with $f = 0.53$, 0.58 and 0.68 from left to right, with a zero surface charge density ($\alpha = 0.89$, 0.72 and 0.47, respectively) and $L = 10$ Å. Corresponding Monte-Carlo snapshots are provided as ESI†.

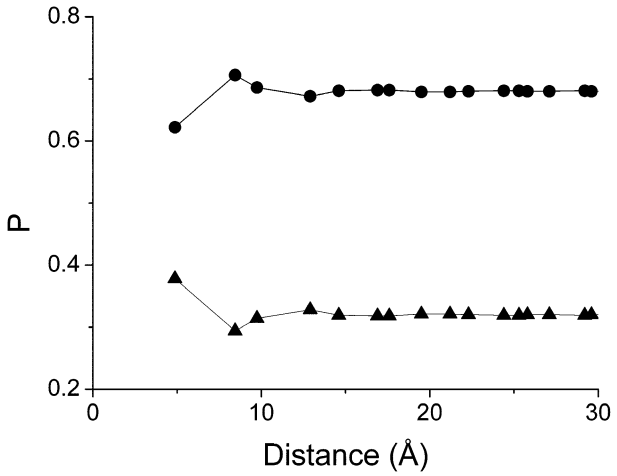

Fig. 8 Pair probability for CTA^+–myristate (triangles) and for myristate–myristate molecules in a myristate–CTA^+ mixture, with $f = 0.69$, $\alpha = 0.45$ ($\Sigma = 0$) and $L = 10$ Å.

the hexagonal lattice. Superstructures are not predicted in this case, even if the Gouy–Chapman length is set to arbitrarily high values. Long-range superstructures are predicted only if several constraints are met:

(1) The composition in $C_{13}D_{27}COO^-$, $C_{13}D_{27}COOH$ and CTA^+ must be topologically compatible with a hexagonal superstructure.

(2) The electrostatic interactions must be high enough, which requires for instance that the screening by the counterions must be small enough (*e.g.* L larger than the mean $C_{13}D_{27}COO^-$–CTA^+ distance).

A hypothetical case where superstructures are predicted corresponds to a 1 : 2 mixture of a monovalent anionic surfactant and divalent cationic surfactant with counterions that mutually neutralize in water. This yields a bilayer with a zero mean charge in contact with a salt-free solution, and therefore first-neighbor interactions of the order of 10 kT.

The impact of the electrostatic interactions on this liquid order has been further tested by introducing HCl in the samples either by direct addition or by preparation with mixtures of CTAOH and CTACl. This equivalently leads to reprotonation of the myristic acid. It has been shown before that this reprotonation is almost quantitative,[36] leading to bilayers with composition $(C_{13}D_{27}COOH)_x(C_{13}D_{27}COO^-)_{1-x}CTA^+$ with $x = Cl^-/CTA^+$. There is therefore no free HCl in solution, the solution can be considered as salt-free and eqn (4) remains valid. Introduction of chloride ions therefore allows increasing the surface charge density of the bilayers without changing the surfactant ratio. At compositions $f = 0.50$ and close to $x = 1$, the bilayers are metastable and crystallize into a 3D crystal of surfactants.[36] However, the lifetime of the metastable lamellar phase is long enough to allow characterization (>4 days).

As the fraction $x = Cl^-/CTA$ increases (Fig. 9, lower panel), there is a decrease of the local in-plane order, as monitored by the amplitude of the peak in the 0.5–1 $Å^{-1}$ region which decreases with respect to the amplitudes of the second harmonic of the form factor ($q = 0.3$ $Å^{-1}$) and of the 110 peak ($q = 1.5$ $Å^{-1}$). This demonstrates that electrostatic interactions contribute to the short-range liquid order of the

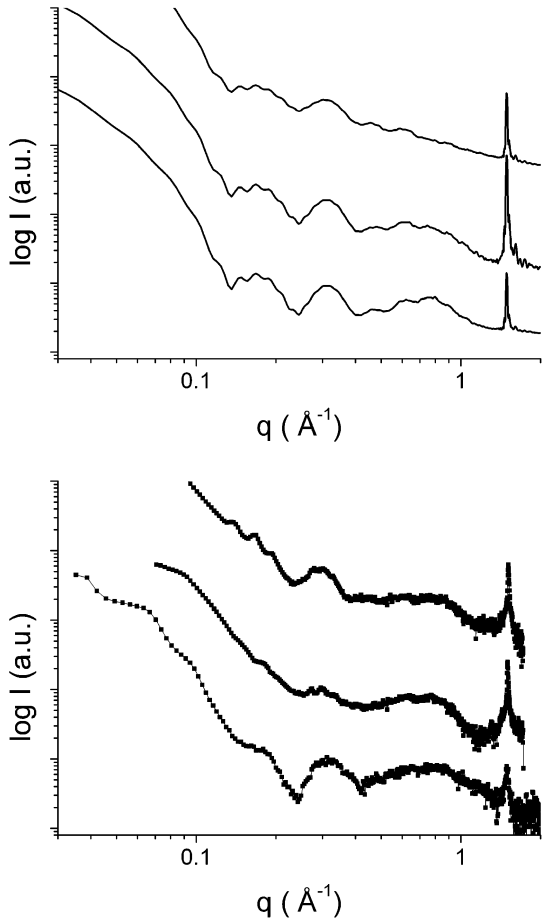

Fig. 9 Monte-Carlo simulations (upper panel) and experimental neutron data (lower panel), with from bottom to top: $f = 0.51$ and $x = Cl^-/CTA = 0.10$, $f = 0.50$ and $x = 0.40$, $f = 0.50$ and $x = 1.00$. The Monte-Carlo simulations were performed with $L = 14.8$ Å, 2.30 Å and 1.0 Å, respectively.

surfactants of opposite charge in the bilayer. However, the amplitude expected from the Monte-Carlo simulations is significantly underestimated with respect to the experimental points (Fig. 9, upper panel). Meanwhile, this loss of local order is limited, as the corresponding correlation peak remains clearly observable even at $x = 1.0$. By contrast, the correlation peak as predicted by the Monte-Carlo simulations completely vanishes at $x = 1.0$. This demonstrates that the electrostatic interactions as determined by eqn (4) are underestimated. Possible adjustments can be the explicit treatment of the counterions instead of a mean-field approach. Other interactions can also contribute to the repulsion between like surfactants, and/or to the attraction between unlike surfactants. Among other possibilities, there is the interaction between surfactant chains, or the formation of a network of hydrogen bonds between carboxylate head groups, as already invoked to account for the rigidity of these bilayers.[4,42–44] However, infrared data are ambiguous and could not provide direct proof yet. Electrostatic interactions participate partially in the local liquid order superimposed on the hexagonal lattice, but the other relevant interactions remain to be determined.

Conclusions

The long-range hexagonal order and the shorter-range liquid order in the lateral distribution of surfactants of opposite charge are, respectively, characterized by a Bragg peak ($q = 1.5$ Å^{-1}) and a broader correlation peak ($q = 0.80$ Å^{-1}). The magnitude of this correlation peak compares well with the prediction of a Monte-Carlo simulation, provided that the oil–water dielectric interface and the dissociation equilibrium of myristic acid are taken into account. Superstructures are not experimentally observed with such surfactants, but minimal conditions for their formation can be formulated. An attenuation of the correlation peak upon addition of HCl is experimentally observed, but this attenuation is overestimated by the Monte-Carlo prediction. Additional or stronger electrostatic interactions are therefore present in the myristate–alkyltrimethylammonium mixtures.

Acknowledgements

The authors are grateful to the Institut Laue-Langevin for the allocation of beamtime on D16 and D22.

Notes and references

1 P. Jokela, B. Jonsson and A. Khan, *J. Phys. Chem.*, 1987, **91**, 3291–3298.
2 C. Tondre and C. Caillet, *Adv. Colloid Interface Sci.*, 2001, **93**, 115–134.
3 E. W. Kaler, K. L. Herrington, A. K. Murthy and J. A. N. Zasadzinski, *J. Phys. Chem.*, 1992, **96**, 6698–6707.
4 T. Zemb, D. Carriere, K. Glinel, M. Hartman, A. Meister, C. Vautrin, N. Delorme, A. Fery and M. Dubois, *Colloids Surf., A*, 2007, **303**, 37–45.
5 J. C. Hao and H. Hoffmann, *Curr. Opin. Colloid Interface Sci.*, 2004, **9**, 279–293.
6 A. Khan and E. F. Marques, *Curr. Opin. Colloid Interface Sci.*, 1999, **4**, 402–410.
7 B. Kronberg, *Curr. Opin. Colloid Interface Sci.*, 1997, **2**, 456–463.
8 S. Segota and D. Tezak, *Adv. Colloid Interface Sci.*, 2006, **121**, 51–75.
9 S. Svenson, *Curr. Opin. Colloid Interface Sci.*, 2004, **9**, 201–212.
10 T. Zemb, O. Tache, F. Ne and O. Spalla, *J. Appl. Crystallogr.*, 2003, **36**, 800–805.
11 B. A. Coldren, H. Warriner, R. van Zanten and J. A. Zasadzinski, *Langmuir*, 2006, **22**, 2465–2473.
12 A. Shiloach and D. Blankschtein, *Langmuir*, 1998, **14**, 1618–1636.
13 L. L. Brasher, K. L. Herrington and E. W. Kaler, *Langmuir*, 1995, **11**, 4267–4277.
14 N. Funasaki and S. Hada, *J. Phys. Chem.*, 1979, **83**, 2471–2475.
15 S. A. Safran, P. Pincus and D. Andelman, *Science*, 1990, **248**, 354–356.
16 G. Vernizzi and M. O. de la Cruz, *Proc. Natl. Acad. Sci. U. S. A.*, 2007, **104**, 18382–18386.
17 M. Dubois, V. Lizunov, A. Meister, T. Gulik-Krzywicki, J. M. Verbavatz, E. Perez, J. Zimmerberg and T. Zemb, *Proc. Natl. Acad. Sci. U. S. A.*, 2004, **101**, 15082–15087.
18 H. T. Jung, B. Coldren, J. A. Zasadzinski, D. J. Iampietro and E. W. Kaler, *Proc. Natl. Acad. Sci. U. S. A.*, 2001, **98**, 1353–1357.
19 H. T. Jung, S. Y. Lee, E. W. Kaler, B. Coldren and J. A. Zasadzinski, *Proc. Natl. Acad. Sci. U. S. A.*, 2002, **99**, 15318–15322.
20 F. E. Antunes, R. O. Brito, E. F. Marques, B. Lindman and M. Miguel, *J. Phys. Chem. B*, 2007, **111**, 116–123.
21 A. Gonzalez-Perez, M. Schmutz, G. Waton, M. J. Romero and M. P. Krafft, *J. Am. Chem. Soc.*, 2007, **129**, 756–757.
22 Y. Michina, D. Carrière, C. Mariet, M. Moskura, P. Berthault, L. Belloni and T. Zemb, *Langmuir*, 2009, **25**, 698–706.
23 D. Kopetzki, Y. Michina, T. Gustavsson and D. Carrière, *Soft Matter*, 2009, DOI: 10.1039/b907339f.
24 S. M. Loverde, Y. S. Velichko and M. O. de la Cruz, *J. Chem. Phys.*, 2006, **124**, 144702.
25 M. M. D. Lim, Y. S. Velichko, M. O. De la Cruz and G. Vernizzi, *J. Phys. Chem. B*, 2008, **112**, 5423–5427.
26 M. E. Amato, E. Caponetti, D. C. Martino and L. Pedone, *J. Phys. Chem. B*, 2003, **107**, 10048–10056.
27 L. L. Brasher and E. W. Kaler, *Langmuir*, 1996, **12**, 6270–6276.
28 J. Penfold, E. Staples and I. Tucker, *Adv. Colloid Interface Sci.*, 1996, **68**, 31–55.
29 P. C. Griffiths, M. L. Whatton, R. J. Abbott, W. Kwan, A. R. Pitt, A. M. Howe, S. M. King and R. K. Heenan, *J. Colloid Interface Sci.*, 1999, **215**, 114–123.
30 H. P. Hentze, S. R. Raghavan, C. A. McKelvey and E. W. Kaler, *Langmuir*, 2003, **19**, 1069–1074.
31 J. C. Hao, H. Hoffmann and K. Horbaschek, *J. Phys. Chem. B*, 2000, **104**, 10144–10153.
32 S. U. Egelhaaf and P. Schurtenberger, *Phys. Rev. Lett.*, 1999, **82**, 2804–2807.
33 B. F. B. Silva, E. F. Marques and U. Olsson, *Langmuir*, 2008, **24**, 10746–10754.
34 M. Bergstrom and J. S. Pedersen, *Phys. Chem. Chem. Phys.*, 1999, **1**, 4437–4446.
35 D. J. Iampietro, L. L. Brasher, E. W. Kaler, A. Stradner and O. Glatter, *J. Phys. Chem. B*, 1998, **102**, 3105–3113.
36 E. Maurer, L. Belloni, T. Zemb and D. Carriere, *Langmuir*, 2007, **23**, 6554–6560.
37 R. R. Netz and H. Orland, *Eur. Phys. J. E*, 2000, **1**, 203.
38 A. Tardieu, V. Luzzati and F. C. Reman, *J. Mol. Biol.*, 1973, **75**, 711–718.
39 G. Forster, A. Meister and A. Blume, *Curr. Opin. Colloid Interface Sci.*, 2001, **6**, 294–302.
40 E. B. Sirota, *Langmuir*, 1997, **13**, 3849–3859.
41 J. S. Pedersen, in *Neutron, X-rays & Light Scattering*, ed. P. Lindner and T. Zemb, North-Holland, Amsterdam, 1991, ch. 16.
42 N. Delorme, M. Dubois, S. Garnier, A. Laschewsky, R. Weinkamer, T. Zemb and A. Fery, *J. Phys. Chem. B*, 2006, **110**, 1752–1758.
43 M. A. Hartmann, R. Weinkamer, T. Zemb, F. D. Fischer and P. Fratzl, *Phys. Rev. Lett.*, 2006, **97**, 018106.
44 N. Delorme, J. F. Bardeau, D. Carriere, M. Dubois, A. Gourbil, H. Mohwald, T. Zemb and A. Fery, *J. Phys. Chem. B*, 2007, **111**, 2503–2505.

